THE POLAR PLASMA WAVE INSTRUMENT

D. A. GURNETT, A. M. PERSOON, R. F. RANDALL, D. L. ODEM,
S. L. REMINGTON, T. F. AVERKAMP, M. M. DEBOWER, G. B. HOSPODARSKY,
R. L. HUFF, D. L. KIRCHNER, M. A. MITCHELL, B. T. PHAM, J. R. PHILLIPS,
W. J. SCHINTLER, P. SHEYKO, and D. R. TOMASH
Department of Physics and Astronomy, The University of Iowa, Iowa City, IA 52242, U.S.A.

(Received 20 June, 1993)

Abstract. The Plasma Wave Instrument on the Polar spacecraft is designed to provide measurements of plasma waves in the Earth's polar regions over the frequency range from 0.1 Hz to 800 kHz. Three orthogonal electric dipole antennas are used to detect electric fields, two in the spin plane and one aligned along the spacecraft spin axis. A magnetic loop antenna and a triaxial magnetic search coil antenna are used to detect magnetic fields. Signals from these antennas are processed by five receiver systems: a wideband receiver, a high-frequency waveform receiver, a low-frequency waveform receiver, two multichannel analyzers; and a pair of sweep frequency receivers. Compared to previous plasma wave instruments, the Polar plasma wave instrument has several new capabilities. These include (1) an expanded frequency range to improve coverage of both low- and high-frequency wave phenomena, (2) the ability to simultaneously capture signals from six orthogonal electric and magnetic field sensors, and (3) a digital wideband receiver with up to 8-bit resolution and sample rates as high as 249k samples s^{-1}.

1. Introduction

The Plasma Wave Instrument (PWI) on the Polar spacecraft is designed to provide comprehensive measurements of plasma waves in the polar regions of the Earth's magnetosphere. The study of plasma waves in the Earth's polar regions has a long history extending over more than half a century. The first reported observation of a high-latitude plasma wave phenomena was in 1933 by Burton and Boardman (1933). Using a telegraph line and a telephone receiver as a simple receiving system, Burton and Boardman discovered that bursts of very-low-frequency (VLF) radio 'static' were sometimes correlated with flashes of auroral light. These observations were confirmed in later studies by Ellis (1957), Dowden (1959), Martin *et al.* (1960), and others using ground-based VLF radio receivers. Typically, the aurora-associated emissions were the strongest in the frequency range from about 1 to 20 kHz. Because the emissions tended to produce a hiss-like sound in the audio output of the radio receiver, they soon became known as 'auroral hiss'.

The launch of the first Earth-orbiting satellites in the late 1950s opened a new era in the study of VLF radio wave phenomena. In addition to auroral hiss, a wide variety of new wave phenomena were quickly discovered in the region of magnetized plasma around the Earth known as the magnetosphere. These waves soon came to be known as 'plasma waves', since they depended on the presence of a plasma for their generation and propagation. In general, plasma waves can

Space Science Reviews **71:** 597–622, 1995.

be divided into two types: electromagnetic and electrostatic. Electromagnetic plasma waves have both electric and magnetic fields and propagate at high speeds, usually much greater than the thermal speeds of the plasma particles, and over long distances, often one Earth radius (R_E) or more. Auroral hiss is an example of an electromagnetic plasma wave emission. Electromagnetic waves in the Earth's magnetosphere can be further subdivided into two types, those that are confined to the immediate vicinity of the Earth, and those that can escape to great distances. The latter are often referred to as planetary radio emissions. These emissions have access to free space and do not require a plasma to propagate. The best known example of a terrestrial radio emission is auroral kilometric radiation (Gurnett, 1974), which is an intense radio emission produced along the Earth's auroral field lines in the frequency range from about 50 to 400 kHz. Electrostatic plasma waves have no magnetic field and propagate at low speeds, on the order of the plasma thermal speeds, and are often strongly damped, thereby severely limiting their range of propagation. The best known examples of electrostatic waves are probably the Langmuir wave (Tonks and Langmuir, 1929), which consists of an electrostatic oscillation near a characteristic frequency known as the electron plasma frequency, and the ion acoustic wave [Stix, 1962], which is similar to a sound wave in an ordinary gas.

A list of some of the most important types of plasma wave emissions observed in the polar regions of the Earth's magnetosphere is given in Table I. This table lists the name of the emission, the mode of propagation, the electromagnetic (EM)/electrostatic (ES) character of the wave, the frequency range, and the generation mechanism. The frequency of the emission is controlled by certain characteristic frequencies of the plasma, the most important of which are the cyclotron frequency

$$f_c = \frac{1}{2\pi}\frac{|e|\,B}{m}\,, \tag{1}$$

and the plasma frequency

$$f_p = \frac{1}{2\pi}\sqrt{\frac{Ne^2}{\epsilon_0 m}}\,, \tag{2}$$

where e and m are the particle charge and mass, B is the magnetic field strength, ϵ_0 is the permittivity of free space, and N is the number density. Separate cyclotron frequencies and plasma frequencies are defined for each species in the plasma. The cyclotron frequencies and plasma frequencies are often combined to form resonance and cutoff frequencies for various wave modes, such as the upper hybrid resonance frequency f_{UHR}, the lower hybrid resonance, f_{LHR}, the right-hand cutoff $f_{R=0}$, and the left-hand cutoff $f_{L=0}$. Formulas for these various frequencies are given at the bottom of Table I. For a further discussion of the relation of these characteristic frequencies to the various plasma wave emissions observed in the Earth's polar regions, see the reviews by Shawhan (1979) and Gurnett (1991).

TABLE I

Plasma wave modes

Name of emission	Electromagnetic (EM) or electrostatic (ES)	Mode of propagation	Frequency range	Generation mechanism
Auroral hiss	EM	Whistler-mode	$f < \min\{f_{ce}, f_{pe}\}$	Electron beam
Auroral kilometric radiation	EM	Free-space $R-X$ modes and $L-O$ modes	$f > f_{R=0}(R-X$ mode) $f > f_{pe}(L-O$ mode)	Electron anisotropy
Electron plasma oscillations	ES	Langmuir mode	$f \simeq f_{pe}$	Electron beam
Z-mode radiation	EM	Z-mode	$f_{L=0} < f < f_{\mathrm{UHR}}$	Electron beam and/or mode coupling
Lower-hybrid noise	ES	LHR mode	$f \sim f_{\mathrm{LHR}}$	Electron beam
Ion acoustic waves	ES	Ion acoustic mode	$f \lesssim f_{pi}$	Current
Electromagnetic ion cyclotron waves	EM	Electromagnetic ion cyclotron mode	$f < f_{ci}$	Electron beam
Electrostatic ion cyclotron waves	ES	Electrostatic ion cyclotron mode	$f \sim n f_{ci}$	Ion-beam

$f_{R=0} = f_{ce}/2 + [(f_{ce}/2)^2 + f_{pe}^2]^{1/2}$; $f_{L=0} = -f_{ce}/2 + [(f_{ce}/2)^2 + f_{pe}]^{1/2}$.
$f_{\mathrm{UHR}} = [f_{ce}^2 + f_{pe}^2]^{1/2}$; $f_{\mathrm{LHR}} = (f_{ce} f_{ci})^{1/2}$.

The importance of plasma waves in the magnetospheric plasma lies in their resonant interactions with charged particles. Two types of resonant interactions can occur between a plasma wave and a charged particle, the Landau resonance and the cyclotron resonance. The Landau resonance occurs when the component of the phase velocity of the wave along the static magnetic field, $\omega/k_{\|}$, matches the particle velocity along the magnetic field (the symbol $\|$ indicates the component parallel to the magnetic field). Cyclotron resonance occurs when the angular velocity of the wave field around the magnetic field matches the angular velocity of the particle, or its harmonic, in a frame of reference moving along the magnetic field with the particle. These resonance conditions can be summarized by the formula

$$v_{\|\mathrm{Res}} = \frac{\omega - n\omega_c}{k_{\|}} , \tag{3}$$

which give the parallel resonance velocity as a function of the frequency, ω, and the wave number, $k_{\|}$. The Landau resonance condition is given by $n = 0$, the first-order cyclotron resonance is given by $n = 1$, and the higher order (harmonic) cyclotron resonances are given by $|n| > 1$.

When a resonant interaction occurs between a plasma wave and a charged particle, energy and momentum is exchanged between the wave and the particle. Which way the energy and momentum flows depends in detail on the distribution of particle velocities. Certain types of distribution functions, such as a beam or a loss cone, lead to wave growth or amplification, whereas others, such as an isotropic distribution, lead to damping. A beam is a region of the velocity distribution function that has a positive slope (i.e., $\partial f/\partial v_{\|} > 0$ for $v_{\|} > 0$), and a loss cone is a conical region in velocity space, aligned along the magnetic field, that is strongly depopulated due to collisions with the atmosphere. In the auroral zone, for example, electron beams accelerated by parallel electric fields are believed to be responsible for the generation of auroral hiss via a Landau resonance (Gurnett, 1966; Gurnett and Frank, 1972; Laaspere and Hoffman, 1976; Maggs, 1976). Auroral kilometric radiation (AKR) is believed to be generated by a loss cone in the auroral electron distribution via a relativistic n = 1 cyclotron resonance mechanism (Wu and Lee, 1979; Winglee, 1985; Zarka *et al.*, 1986; Louarn *et al.*, 1990). One consequence of wave growth, particularly for cyclotron interactions, is that particles are scattered into the loss cone. For charged particles trapped in planetary magnetospheres, scattering into the loss cone is the primary mechanism by which particles are lost from the radiation belts (Kennel and Petschek, 1966). Once generated all internally confined waves must eventually be damped. If the damping involves a resonant interaction, some of the particles can be accelerated to high energies. Such resonant acceleration processes are believed to be the primary mechanism by which nonthermal particle distributions known as conics are generated in the Earth's auroral zones (Shelley and Collin, 1991).

One of the primary objectives of the International Solar Terrestrial Program, of which the Polar spacecraft is a part, is to 'understand the physical processes

controlling the origin, entry, transport, storage, acceleration, and loss of plasmas in the Earth's neighborhood' (Final Report of the Science Definition Working Group, April 1979). Since plasma waves clearly play an important role in the loss and acceleration of plasmas in the Earth's polar regions, it is important that the spectrum of plasma waves be adequately characterized by the Polar spacecraft. This is the primary purpose of the Polar plasma wave investigation. The general objectives of the investigation, as outlined in the proposal submitted to NASA for the Polar plasma wave investigation (Gurnett *et al.*, 1988) are

– to measure the spectral and wave vector characteristics of naturally occurring electromagnetic and electrostatic plasma waves,

– to measure the spectral and wave vector characteristics of electromagnetic and electrostatic waves generated by ground-based active experiments,

– to analyze the plasma wave measurements in collaboration with other Polar investigators, and

– to participate in coordinated studies with other ISTP spacecraft.

The advanced design of the Polar plasma wave instrument and the other instruments on the Polar spacecraft will allow us to investigate many specific questions that have been left unanswered. For example, to understand the exact mechanisms involved in the generation of auroral kilometric radiation, closely coordinated wave and plasma measurements must be made as the spacecraft crosses the auroral field lines. It is not known, for example, whether a loss-cone (Wu and Lee, 1979) or an electrostatically trapped particle distribution (Louarn *et al.*, 1990) is responsible for the growth of the auroral kilometric radiation. The high-resolution plasma measurements on Polar, in conjunction with the very detailed plasma wave measurements, should allow us to answer questions of this type. A list of the investigators and institutions participating in this investigation is given in Table II.

2. Desired Instrument Characteristics

Since plasma waves can be either electromagnetic or electrostatic, it is important that both the electric field and magnetic field of a wave be measured in order to distinguish these two types of waves. The frequency range that must be measured is determined by the characteristic frequencies of the plasma. At the high-frequency end of the spectrum, the highest frequencies of interest are determined by the electron plasma frequency, f_{pe} and electron cyclotron frequency, f_{ce}. These frequencies are largest near perigee, and for the nominal Polar perigee radial distance of 1.8 R_E are about 100 to 300 kHz. To make certain that the instrument can cover the spectrum of auroral kilometric radiation, which sometimes extends above 500 kHz, it was decided that the instrument must provide measurements up to 800 kHz. At the low-frequency end of the spectrum, the lowest frequencies of interest are mainly determined by the ion cyclotron frequency, f_{ci}. The ion cyclotron frequencies are smallest near apogee, and for the nominal polar apogee radial distance of 9 R_E are

TABLE II

Polar plasma wave investigation investigators

Investigator	Role	Institution
D. A. Gurnett	PI	University of Iowa
R. R. Anderson	Co-I	University of Iowa
W. S. Kurth	Co-I	University of Iowa
R. W. Fredricks	Co-I	TRW
U. S. Inan	Co-I	Stanford University
L. R. O. Storey	Co-I	Goddard Space Flight Center
M. L. Kaiser	Co-I	Goddard Space Flight Center
M. C. Kelley	Co-I	Cornell University
P. M. Kintner	Co-I	Cornell University
H. Matsumoto	Co-I	Kyoto University
M. Temerin	Co-I	University of California, Berkeley
B. T. Tsurutani	Co-I	Jet Propulsion Laboratory

about 1.5 Hz for H^+ ions, and about 0.1 Hz for O^+ ions. To provide measurements near the ion cyclotron frequency, it was decided that the instrument must provide measurements down to 0.1 Hz. This low-frequency limit provides some overlap with the static electric field (EFI) and the magnetometer (MAG) instruments which provide quasi-static electric and magnetic field measurements at frequencies up to several tens of Hz.

One of the more difficult decisions that must be made in the design of any plasma wave instrument is the choice of the frequency and time resolution. Our approach has been to provide several different types of receivers, each of which has certain advantages in time and frequency resolution. For example, a sweep frequency receiver is included that has very good frequency resolution (few percent) but relatively poor time resolution (few tens of seconds). To provide improved time resolution, a multichannel analyzer is also included that has very good time resolution ($\sim$ 1 s) but relatively poor frequency resolution (4 channels per decade). To provide the highest possible frequency-time resolution, a wideband receiver is included that provides essentially continuous waveforms over a broad bandwidth (up to 90 kHz). However, since the wideband system generates extremely high data rates (249 kbits/s^{-1}), wideband waveform data can only be transmitted a small fraction of the time ($\sim$ 15%).

To determine the direction of propagation of electromagnetic and electrostatic waves, it is essential that simultaneous 3-axis electric and magnetic field measurements be obtained. Since broadband multi-axis measurements also imply very high data rates, it was decided that these measurements could be obtained on a sampled basis, since continuous wave normal and Poynting flux measurements are not necessary to provide a good understanding of the wave fields.

3. Electric and Magnetic Field Antennas

The Polar PWI uses seven antennas for detecting the electric and magnetic field components of plasma waves. Detailed characteristics of the electric and magnetic antennas are listed in Table III. These antennas consist of a pair of orthogonal two-sphere electric antennas in the spin plane of the spacecraft with sphere-to-sphere separations of 130 m (E_u) and 100 m (E_v), respectively, a short two-sphere electric antenna (E_z) aligned along the spacecraft spin axis with a sphere-to-sphere separation of 14 m, a triaxial search coil magnetic antenna system mounted on the end of a 6-m rigid boom, and a magnetic loop antenna mounted on the same boom with its axis oriented parallel to the E_u electric antenna. The mounting arrangement of the antennas on the spacecraft is illustrated in Figure 1.

The electric field antennas and associated electronics are provided by the Electric Field Instrument (EFI) team, and are used by both PWI and EFI. The spheres on the electric antennas are 8 cm in diameter and contain high-impedance preamplifiers that provide signals to the main electronics package. (For a detailed description of the EFI antennas, see Harvey *et al.* (1994).) Buffer amplifiers in the deployment mechanisms provide independent signals to EFI and PWI. Each of the three search coil antennas consists of two coils mounted on a high-permeability μ-metal rod 40 cm long. Each coil consists of 10,000 turns of No. 40 AWG wire. The voltage from the coils is amplified by a preamplifier to provide a low-impedance signal to the main electronics box. The preamplifiers are mounted in the search coil housing. The sensitivity constant of the search coil is 70 μV/nT–Hz and the resonance frequency is approximately 8 kHz. The axes of the B_u, B_v, and B_z sensors are oriented within one degree of the E_u, E_v, and E_z electric antenna axes. A photograph of one of the Polar search coil antennas is shown in Figure 2. The search coil antenna design is based on similar sensors flown on the ISEE 1 and 2 spacecraft. The loop antenna is similar to the magnetic loop antenna flown on the Dynamics Explorer 1 spacecraft and is designed to detect magnetic fields over a frequency range from 25 Hz to 800 kHz. The loop sensitivity constant is 110 μV/nT–Hz and the resonance frequency is approximately 50 kHz. A photograph of the magnetic loop antenna is shown in Figure 3.

4. Main Electronics Package

A block diagram of the main electronics package and the associated system of sensors is shown in Figure 4. The instrumentation in the main electronics package consists of five receiver systems: a high-time resolution multichannel analyzer (MCA); a narrowband sweep frequency receiver (SFR); a high-frequency waveform receiver (HFWR); a low-frequency waveform receiver (LFWR); and a wideband receiver (WBR). The detailed characteristics of these receiver systems are listed in Table IV. The receivers can be connected to the electric and magnetic antennas in various

TABLE III

PWI antenna characteristics

Electric dipole antenna (E_u)	
Frequence range	DC to 1.25 MHz
Construction	Two 8-cm diameter spheres with a sphere-to-sphere separation of 130 m
Location	Deployed in the spin plane
Effective electrical length	130 m
Manufacturer	University of California, Berkeley
Electric dipole antenna (E_v)	
Frequency range	DC to 1.25 MHz
Construction	Two 8-cm diameter spheres with a sphere-to-sphere separation of 100 m
Location	Deployed in the spin plane, perpendicular to E_u
Effective electrical length	100 m
Manufacturer	University of California, Berkeley
Electric dipole antenna (E_z)	
Frequency range	DC to 1.25 MHz
Construction	Two 8-cm diameter spheres mounted on rigid stacer booms providing a sphere-to-sphere separation of 14 m
Location	Deployed along the spin axis
Effective electrical length	14 m
Manufacturer	University of California, Berkeley
Magnetic loop antenna	
Frequency range	25 Hz to 50 kHz responds to dB/dt; 50 kHz to 800 kHz responds to B
Construction	Single loop of aluminum tubing, 1.0 m^2 area
Sensitivity constant	Integral secondary transformer and preamplification giving 110 μV/nT–Hz
Location	Mounted on 6 m boom, oriented parallel to the E_v electric antenna
Manufacturer	University of Iowa
Heritage	Similar to Dynamics Explorer-A unit
Trixaxial search coil magnetic antennas	
Frequency range	0.1 Hz to 8 kHz responds to dB/dt; 8 kHz to 50 kHz responds to B
Construction	Three orthogonal coils, each with 20,000 turns of No. 40 wire on a 40 cm high-permeability μ-metal rod enclosed in Vespel housing coated with silver conducting paint and vacuum-deposited aluminum.
Sensitivity constant	Preamplificaton giving 70 μV/nT-Hz.
Location	Mounted on 6 m boom, measured from the shell of the spacecraft.
Manufacturer	University of Iowa.
Heritage	Similar to ISEE-1 and ISEE-2 units.

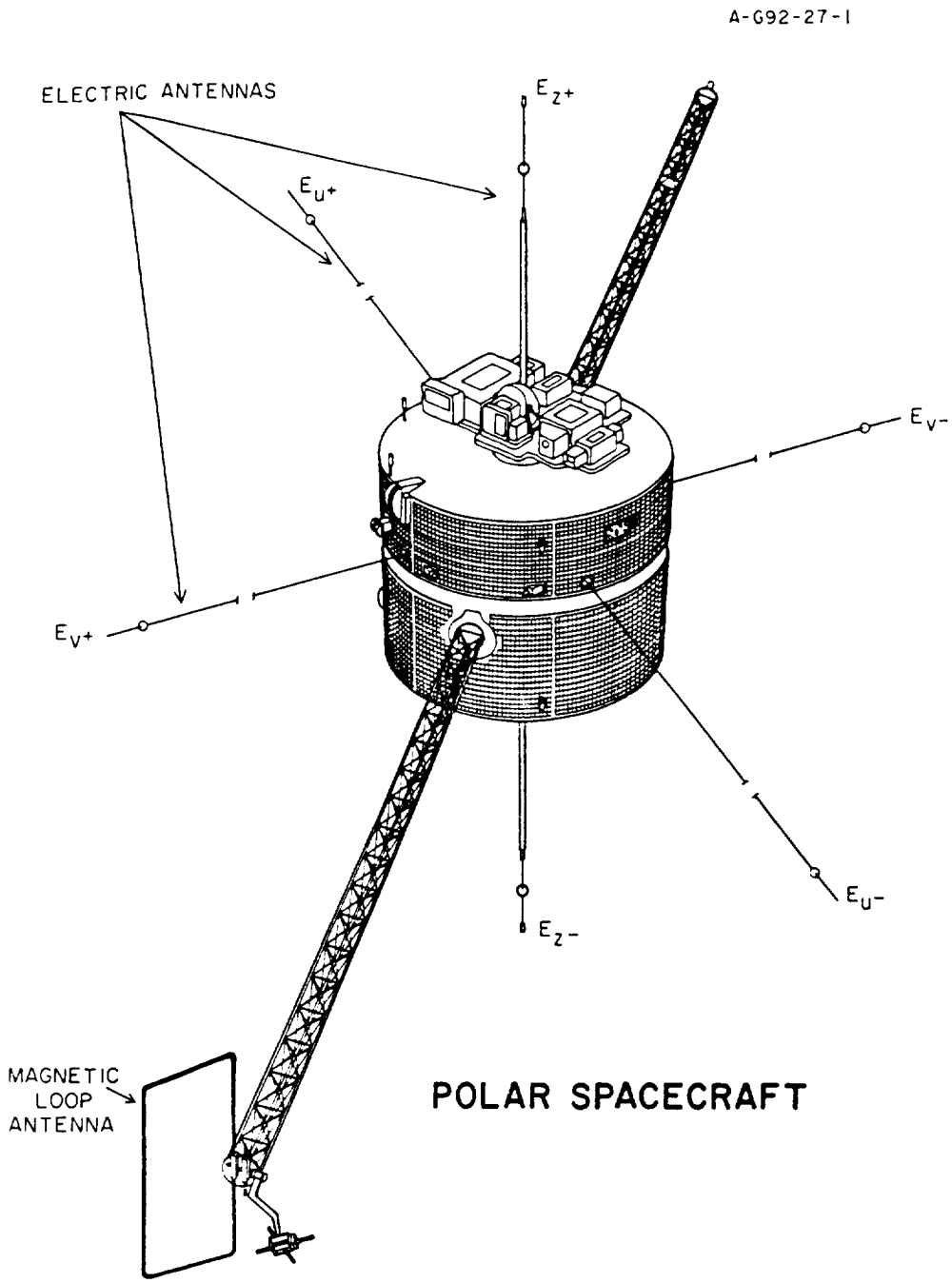

Fig. 1. A schematic drawing of the Polar spacecraft, illustrating the orientation of the three orthogonal electric antennas, the magnetic loop antenna, and the triaxial search coil antennas.

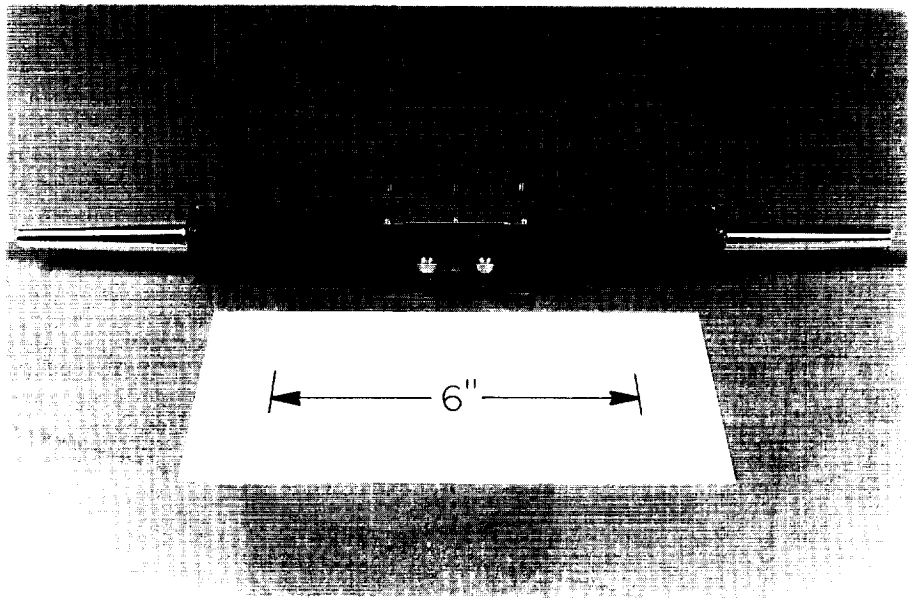

Fig. 2. A photograph of a magnetic search coil antenna.

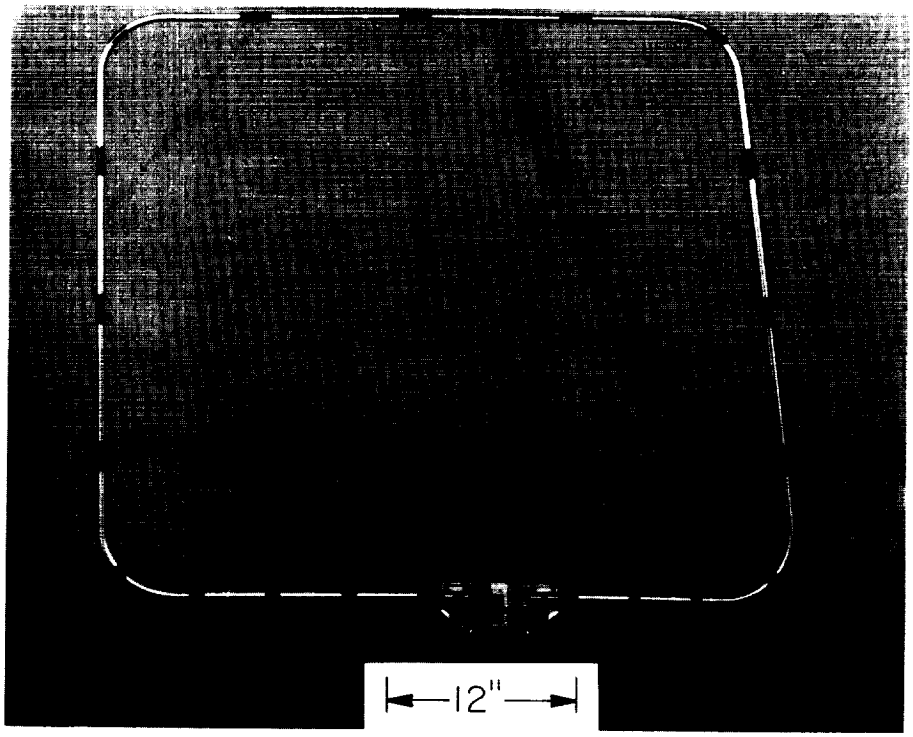

Fig. 3. A photograph of the magnetic loop antenna.

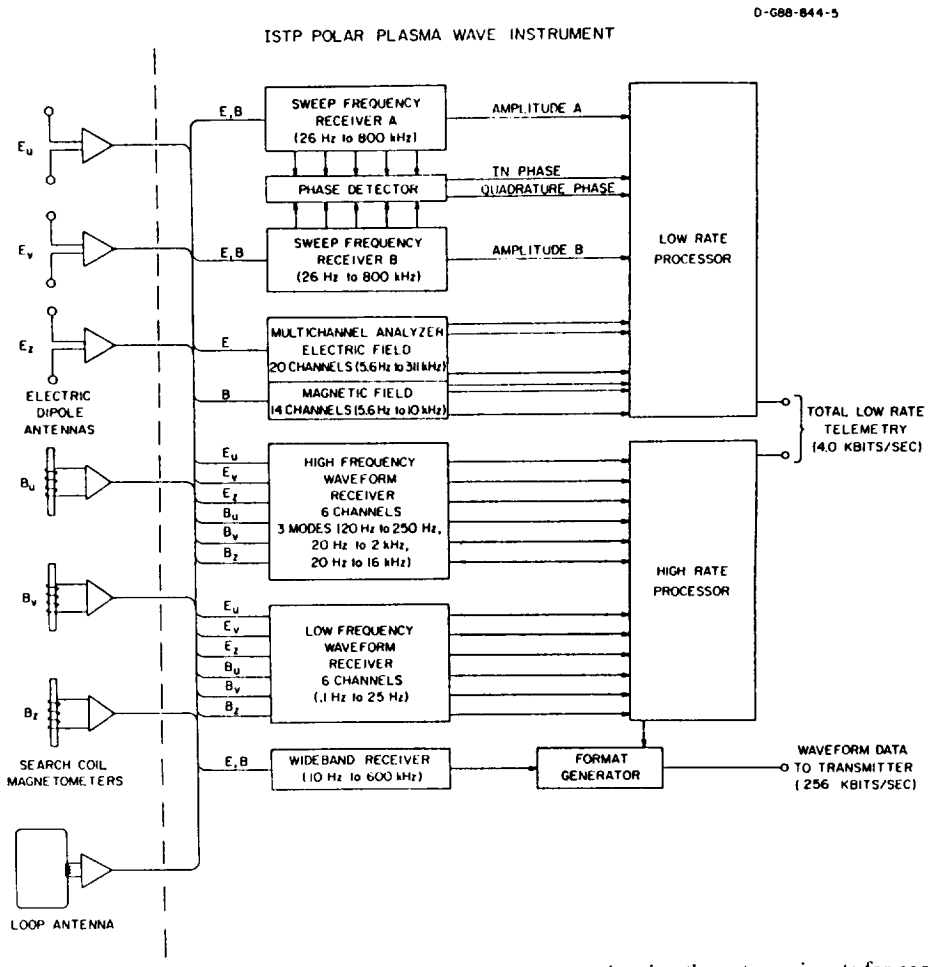

Fig. 4. A block diagram of the Polar Plasma Wave Instrument, showing the antenna inputs for each of the five receiver systems and the path of the data outputs from the receivers through the digital processing units.

combinations by antenna selection switches as listed in Table IV. The sampling of the outputs from the various receiver systems is controlled by two microprocessor-based digital processing units. The Low-Rate Processor (LRP), which uses an 8085 microprocessor, is used to process signals from the SFR and MCA. The High-Rate Processor (HRP), which uses an 8086 microprocessor, is used to perform digital filter operations on data from the LFWR and HFWR. The HRP controls the operation of the WBR and includes a 3.4-megabit waveform capture memory for storage of the HFWR and LFWR waveform data. The LRP and HRP have independent data connections to the spacecraft to prevent complete disruption of the data output due to processor upsets. A photograph of the main electronics package is given in Figure 5.

TABLE IV
PWI receiver characteristics

Multichannel Analyzer (MCA)	
Frequency range	Electric MCA: 5.6 Hz–311 kHz
	Magnetic MCA: 5.6 Hz–10 kHz
Frequency resolution	Electric MCA: 20 log-spaced channels
	Magnetic MCA: 14 log-spaced channels
	4 frequency channels/decade with 15% bandwidth below 10 kHz and 7.5% bandwidth at 10 kHz and above
Time resolution	1.3 s/spectra
Dynamic range	100 dB
Sensors	Electric MCA: E_u, E_v, E_z, and magnetic loop antenna
	Magnetic MCA: E_u and the magnetic search coil antennas (B_u, B_v, B_z).
Technique	Two receivers with parallel filtering and detection channels.
	Amplitude derived from 100 dB high-frequency log compressors.
Heritage	Similar to ISEE-1 electric and magnetic spectrum analyzers.
Step Frequency Receiver (SFR)	
Frequency range	5 frequency bands: 26–200 Hz, 0.2–1.6 kHz, 1.7–12.6 kHz, 13–100 kHz, 100–808 kHz, simultaneously for two receivers.
Frequency resolution:	Log Mode: 64 frequency steps (two highest bands) and 32 frequency steps (three lowest bands) log-spaced 26 Hz–808 kHz; 5% bandwidth for the lowest frequency band and 1% bandwidth for the four highest frequency bands.
	Linear Mode: 128 frequency steps (two highest bands) and 64 frequency steps (three lowest bands) linearly-spaced 26 Hz–808 kHz; Δf is constant for each frequency band
Time resolution	Log Mode: 32 s/spectra
	Linear Mode: 64 s/spectra
Dynamic range	100 dB
Phase resolution	± 1 deg phase
Sensors	Any pairs from E_u, E_v, E_z, magnetic loop and B_z search coil antenna
Technique	Two double-conversion, single-sideband step frequency receivers driven by common frequency synthesizers under the control of the Low-Rate Data Processing Unit. Amplitude derived from 100 dB logarithmic compressor amplifiers. Waveforms are correlated in EXOR circuits to give in-phase and quadrature phase correlation products.
Heritage	Similar to ISEE-1 SFR receiver.
High-frequency Waveform Receiver (HFWR)	
Frequency range	20 Hz–250 Hz (digital filter)
	20 Hz–2 kHz (digital filter)
	20 Hz–16 kHz (digital filter)
	20 Hz–25 kHz (analog filter)
HFRW sampling rates	558 Hz for 250 Hz filter
	4.46 kHz for 2 kHz filter
	35.71 kHz for 16 kHz filter
	71.43 kHz for 25 kHz filter

Table IV (continued)

Frequency resolution	For the 250 Hz and 2 kHz low-pass filters, approximately 2.2 Hz. For the 16 kHz low-pass filter, approximately 17.4 Hz (Frequency resolution limited by FFT).
Time resolution	$\Delta f \Delta t \approx 1$
Dynamic range	72 dB of dynamic range from the A/D converters, adjusted up to 102 dB by programmable gain amplifiers.
Sensors	The three orthogonal electric antennas E_u, E_v, E_z and the triaxial search coil antennas B_u, B_v, B_z
HFWR H-rate mode	High-Rate Waveform Mode: HFWR data is put into the high-rate telemetry link in place of the wideband data to allow 'fast' 9.2-s waveform capture in the raw data mode
Interferometry mode	Two of the channels are direclty connected to the E_v+ and E_v- antennas to allow digitization of the single-ended waveform.
Technique	Six parallel channels, each consisting of three programmable amplifiers, a low-pass filter and an A/D converter, are clocked simultaneously to provide digitized phase coherent waveform data.
Heritage	New design by University of Iowa.
Low-Frequency Waveform Receiver (LFWR)	
Frequency range	0.1–25 Hz
Sampling rate	100 samples s^{-1}
Frequency resolution	6 filters with a bandwidth of approximately 0.2 Hz
Time resolution	$\Delta f \Delta t \simeq 1$
Dynamic range	72 dB
Sensors	The three orthogonal electric antennas E_u, E_v, E_z and the triaxial search coil antennas B_u, B_v, B_z
Technique	6 parallel, lowpass filters receive signals from buffer amplifiers. The signals are band-limited to 25 Hz and sampled by a 12-bit A/D converter.
Heritage	Similar to Dynamics Explorer-A Quasi-Static Electric Field Measurement System.
Wideband Receiver (WBR)	
Frequency range	Selection of 11, 22, or 90 kHz bandwidths with lower band edge at 0, 125, 250 or 500 kHz
Sample rate	See Table VI
Frequency resolution	Typically 75 Hz. Limited by FFT.
Time resolution	$\Delta f \Delta t \simeq 1$
Compression modes	1, 4, or 8-bit resolution modes which adjust the duty cycle in conjunction with the selected bandwidth to produce a constant output bit rate.
Dynamic range	In the 8-bit mode, 48 dB instantaneous dynamic range. In the 4-bit mode, 24 dB dynamic range. Programmable discrete gain amplifiers provide an A/D dynamic range of 0–75 dB, with 5 dB resolution.
Sensors	Any of E_u, E_v, magnetic loop and B_u search coil antennas.
Optional mode	Three narrowband filters, 1–3, 3–6, and 10–16 kHz, to support ground-based transmitter operations.
Technique	Signals are bandpass filtered with three available bandwidths and four possible base frequencies. Three narrowband filters are also available. The data is formatted into a digital data stream from the A/D converter in three possible compression modes and telemetered to a ground tracking station.
Heritage	Similar to Voyager, ISEE, and Galileo units.

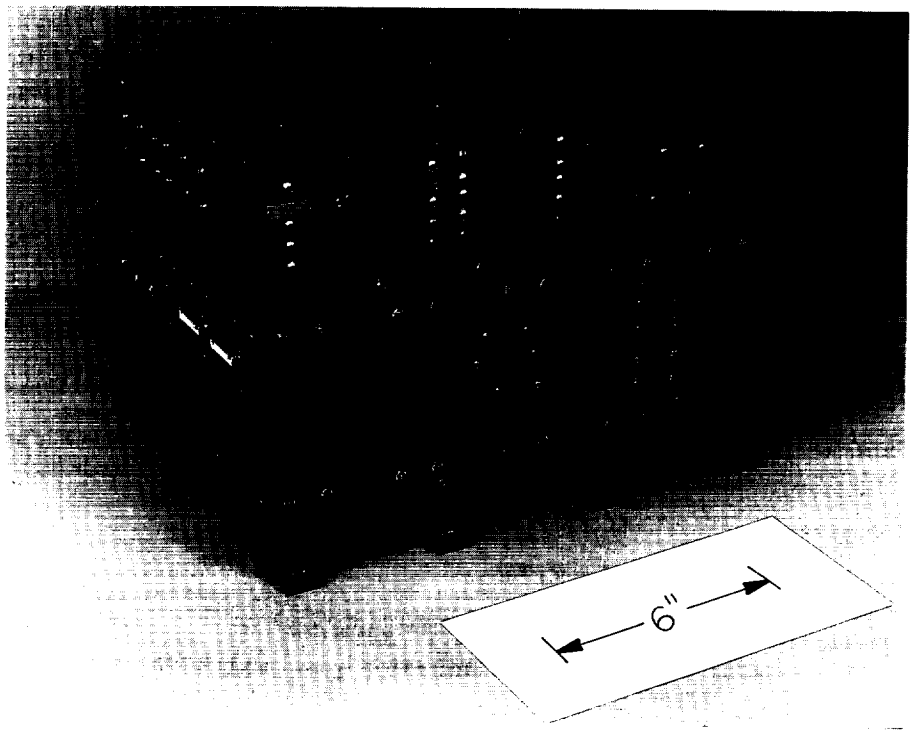

Fig. 5. A photograph of the main PWI electronics package.

The detailed functions of the various receiver systems in the main electronics package are as follows.

The *Multichannel Analyzer* (MCA) is designed to provide good time resolution with relatively poor frequency resolution. The MCA consists of two spectrum analyzers, one for electric field measurements and the other for magnetic field measurements. The electric MCA consists of 20 channels covering the frequency range from 5.6 Hz to 311 kHz. The magnetic MCA consists of 14 channels covering the frequency range from 5.6 Hz to 10 kHz. These analyzers have relatively coarse frequency resolution (4 frequency channels per decade), but very good time resolution. Above 56 Hz, the averaging time constant is 50 ms. Below 56 Hz, the averaging time constant increases as the inverse of the bandwidth. Below 10 kHz, the channel bandwidths are $\pm 15\%$ of the center frequency of each channel. Above 10 kHz, the bandwidths are $\pm 7.5\%$ of the center frequency of each channel. The center frequencies and bandwidths of the electric MCA and the magnetic MCA channels are identical. The dynamic range of the MCA is approximately 100 decibels (dB). All channels are sampled simultaneously so that the electric-to-magnetic field ratios can be accurately compared. The MCA amplitude output is a 0–5 V DC voltage that is proportional to the logarithm of the field strength. In

TABLE V
Design features of the sweep frequency receivers

Band	Frequency range	Bandwidth	Dwell time	Response time	No. frequency steps	
					Log mode	Linear mode
1	24–200 Hz	5 Hz	1.03 s	1 s	32	64
2	200–1600 Hz	15.6 Hz	515.2 ms	382 ms	32	64
3	1.6–12.5 kHz	125 Hz	257.6 ms	177 ms	32	64
4	12.5–100 kHz	1.0 kHz	36.8 ms	24 ms	64	128
5	100–800 kHz	8.0 kHz	36.8 ms	14 ms	64	128

the normal mode of operation, the analyzer outputs are sampled by the Low-Rate Processor at a rate of approximately one sample every 1.3 s. Higher sample rates can be obtained in special modes of operation.

The *Sweep Frequency Receiver* (SFR) is designed to provide good frequency resolution with relatively poor time resolution. The SFR consists of two single-sideband, phase matched, double- conversion receivers in parallel, with both amplitude and phase-measuring capability. The SFR provides amplitude and phase measurements in five frequency bands from 26 Hz to 808 kHz. Each receiver can be connected to one of four sensors (see Table IV).

The SFR has two operating modes, the log step mode and the linear step mode. The log step mode has 64 frequency steps in the two highest frequency bands and 32 frequency steps in the three lowest frequency bands. The linear step mode has 128 frequency steps in the two highest frequency bands and 64 frequency steps in the three lowest frequency bands.

In each of the five frequency bands, the frequency channels can be either logarithmically spaced (log step mode) or linearly spaced (linear step mode). In the log step mode, the frequency resolution varies from approximately 8% at 26 Hz to 3% at 800 kHz. The SFR sequentially advances through the frequency spectrum. In the lowest frequency band, 24–200 Hz, a full frequency spectrum can be obtained every 33 s in the log mode and every 66 s in the linear mode. Because of the wider bandwidths and hence faster response times, the higher frequency bands have faster sweep rates. From 12.5 to 800 kHz, a full frequency spectrum can be obtained every 2.4 s in the log mode and every 4.7 s in the linear mode. The frequency range, the dwell time on each frequency step, and the number of frequency steps for the five frequency bands are listed in Table V for both log and linear modes. Also listed in this table are the response times for SFR bands. The response time is the time for the output of the filter/compressor system to rise from a zero-level output to within 2 dB of the maximum possible output.

The SFR amplitude output is a 0–5 V DC voltage that is proportional to the logarithm of the signal strength over the 100 dB dynamic range of the instrument.

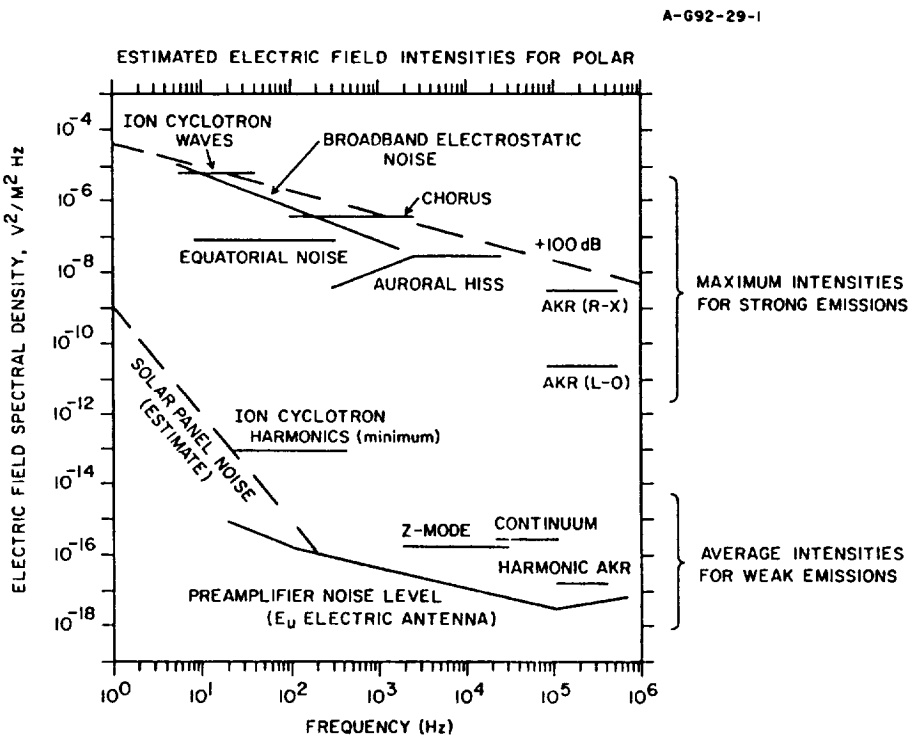

Fig. 6. A plot showing the dynamic range of the PWI and the expected electric field spectral densities for a variety of plasma wave phenomena to be measured by PWI. The estimated spectral densities were derived using plasma wave measurements from the Dynamics Explorer Plasma Wave Instrument. The noise level of the Polar electric antenna was derived from signal sensitivity measurements of the electric antenna preamplifiers and boom buffers, supplied by EFI.

This output is sampled by the Low-Rate Processor. The dynamic range of the instrument and the maximum expected electric and magnetic field spectral densities for a variety of plasma wave phenomena are plotted in Figures 6 and 7. The estimated electric and magnetic field spectral densities were derived from plasma wave measurements on the Dynamics Explorer 1 spacecraft.

Phase measurements are obtained by correlating the frequency converted outputs of the two parallel SFR receivers. In-phase and quadrature correlations are obtained. Using ground processing, the in-phase and quadrature measurements can be used to determine the phase between signals on any two selected antennas. The accuracy of the phase measurement is approximately one degree. Phase measurements can be used to determine the wave polarization and propagation direction.

The *High-Frequency Waveform Receiver* (HFWR) is designed to deliver an instantaneous three-axis snapshot of the electric and magnetic wave fields in one-second waveform segments. These waveforms can be used to determine the wave

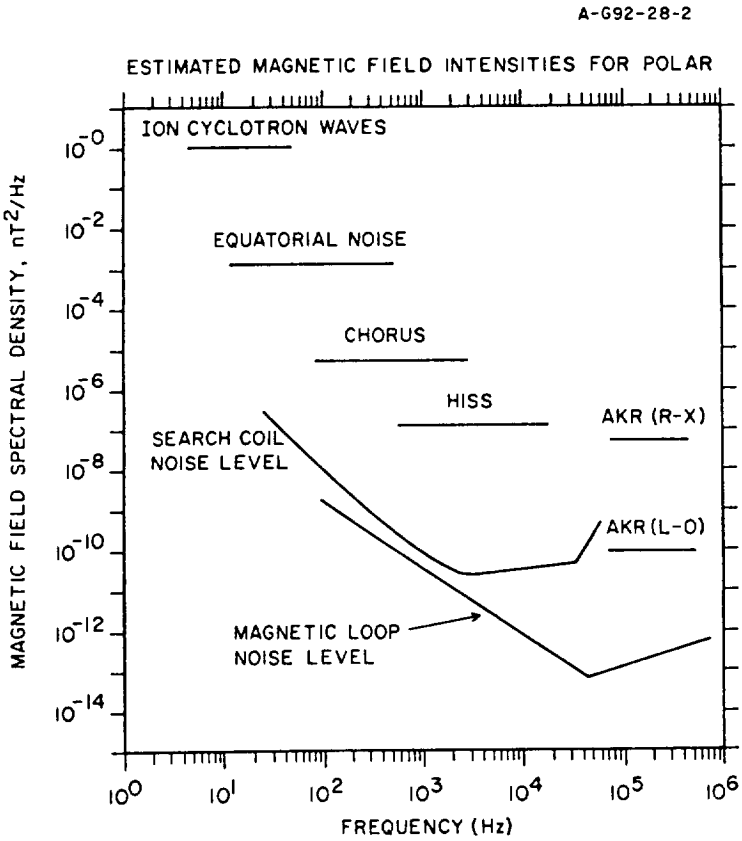

Fig. 7. A plot showing the estimated noise levels for the Polar search coil and magnetic loop antennas and the expected magnetic field spectral densities for a variety of plasma wave phenomena to be measured by PWI. The estimated spectral densities were derived using plasma wave measurements from the Dynamics Explorer Plasma Wave Instrument. The noise levels of the Polar magnetic antennas were derived from noise sensitivity tests conducted at the Goddard Space Flight Center Magnetic Test Facility.

normal direction and Poynting flux. The HFWR consists of six parallel channels connected to the three orthogonal electric field sensors and the triaxial search coil magnetometer. The relative phase of the input signals is preserved by using phase-matched filters and the same sampling signal for each channel. The output waveforms are digitally sampled using a 12-bit analog-to-digital converter to give a dynamic range of 72 dB. Programmable gain amplifiers with gain steps of 15 dB are used to increase the total dynamic range to 102 dB. Gain updates are initiated by the HFWR software at upper and lower trip points. In the default mode of operation, the upper trip point is set 10 dB below the receiver saturation level. The lower trip point is set 20 dB below the upper trip point. The HFWR gain is updated with each complete waveform capture on all 6 channels. The gain may also be selected manually.

Waveform segments up to one second long are captured in a frequency range from 20 Hz to 25 kHz. In the 16-kHz default mode, a complete waveform is captured on all 6 channels and digitally filtered with an upper frequency cutoff of 16 kHz. The duty cycle is 129 s. The phase accuracy of the waveforms is one degree, and the amplitude accuracy is 0.1 dB. On-board digital filtering is used in the High-Rate Processor to synthesize low-pass filters with bandwidths of 250 Hz, 2 kHz and 16 kHz. During ground processing, FFTs are performed on these waveforms to provide the relative phase and amplitude of signals from the various sensors.

The HFWR can be set to sample any one or a combination of input sensors. The E_v and E_z inputs can be switched to single-ended E_v+ and E_v- input signals, allowing interferometry analysis of the signals from these sensors.

The *Low-Frequency Waveform Receiver* (LFWR) is designed to provide an extension of the High Frequency Waveform Receiver into the frequency range below 25 Hz. The LFWR consists of six parallel low-pass filters connected to the three orthogonal electric field sensors and to the triaxial search coils. The input signals are band limited to a frequency range from 0.1 to 25 Hz and are sampled by a 12-bit analog-to-digital converter. The six LFWR channels are sampled simultaneously at a rate of 100 samples s^{-1}. The dynamic range of the LFWR is approximately 72 dB with fixed gain.

The *Wideband Receiver* (WBR) is designed to transmit digitized wideband waveform data from a single antenna with very high frequency-time resolution. The WBR has three normal modes of operation with bandwidths of 11, 22, and 90 kHz. In addition, three narrowband filters, 1–3 kHz, 3–6 kHz, and 10–16 kHz, can be used to support the analysis of ground VLF transmitter signals. In addition to the bandwidth selection, a frequency conversion scheme can be used to shift the frequency range of the WBR to any one of four frequency ranges with base frequencies of 0, 125, 250, and 500 kHz.

The WBR has three analog-to-digital conversion modes with 1-, 4-, and 8-bit resolution. Each mode adjusts the duty cycle in conjunction with the selected bandwidth to produce a constant output bit rate of 249 kilobits per second (kb s^{-1}) to the telemetry system. The default mode of the WBR is the 11-kHz bandwidth at baseband (0 kHz) with 8-bit conversion, which gives a 100% duty cycle. The conversion modes, sample rates and corresponding duty cycles for the three normal mode filters are listed in Table VI.

In the 8-bit mode, the WBR has an instantaneous dynamic range of 48 dB. In the 4-bit mode, the WBR has a dynamic range of 24 dB. Programmable discrete gain amplifiers with a range of 75 dB in 5 dB increments are used in conjunction with the software in the High-Rate Processor to provide an automatic gain control. Gain updates are initiated by the WBR software at upper and lower trip points. In the WBR default mode of operation, the upper trip point is set 10 dB below the receiver saturation level, and the lower trip point is set 12 dB below the upper trip point. In the 11 kHz default mode, the gain state is updated every 0.11 s, although

TABLE VI
Normal survey modes of the wideband receiver

Filter	Sample rate	Duty cycle		
		8 bit	4 bit	1 bit
90 kHz	249 kHz	12.5%	25%	100%
22 kHz	62.25 kHz	50%	100%	
11 kHz	31.12 kHz	100%		

this update rate can be modified by the WBR software. The wideband waveform output and the gain state information are formatted into a digital data stream and telemetered to the ground at 256 kb s^{-1}.

5. Instrument Calibration

An extensive series of amplitude calibrations, frequency responses, and instrument performance checks were carried out for the PWI before integration on the spacecraft. In addition, phase calibrations were performed on the HFWR, LFWR, and SFR receivers.

5.1. Amplitude Calibrations

Amplitude calibrations for each of the receivers were accomplished by providing an input signal of fixed frequency at the center frequency of each filter. The amplitude of the stimulus was decreased in 2 dB increments to cover the full amplitude range of the receiver. The amplitude response curves are used to construct look-up tables that convert the telemetry data value to the true input signal strength. For the WBR and HFWR, the amplitude response tests were repeated for every possible gain setting and for every filter and conversion mode. Using a gain setting of 0 as the baseline, the gain of the input signals for the remaining gain settings was correspondingly decreased to maintain a constant signal strength into the instrument.

The MCA and SFR channels use a compressor with a piecewise-linear approximation to a logarithmic amplitude response. Over the full range of amplitudes, the response of each compressor consists of a series of five distinct linear segments that deviate somewhat from a true logarithmic response. Because the compressors have different amplitude sensitivity characteristics, the amplitude response of each compressor must be individually measured. The amplitude response of a typical logarithmic compressor is shown in Figure 8 for the middle step of the first SFR band at 69 Hz. The slight deviation from a true logarithmic response is caused by

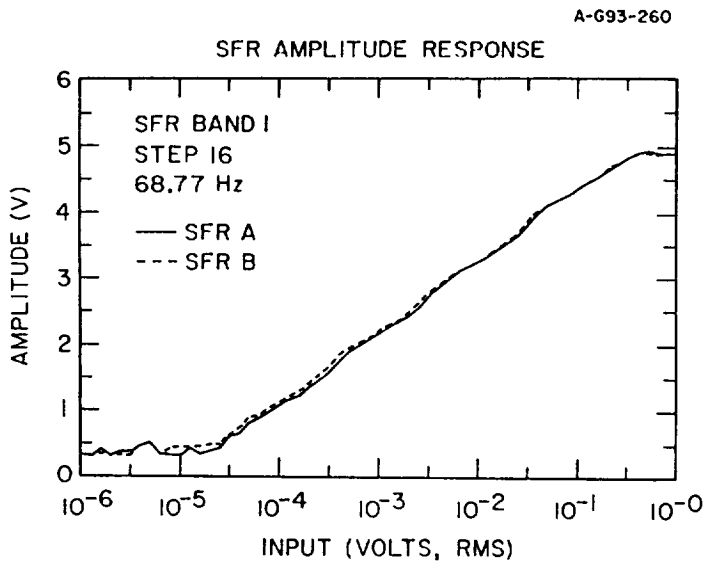

Fig. 8. The amplitude response calibration curve for the middle step of the first SFR band at 69 Hz. The curve illustrates the five-stage, piecewise-linear response of the SFR logarithmic compressor. Amplitude calibration curves for the PWI filters are used to construct look-up tables which convert the telemetry data values to the true input signal strength.

the piecewise-linear response. Similar amplitude responses are measured for the middle frequency step of each SFR band and for the 20 MCA channels.

Since all of the frequency steps of a given SFR band utilize the same logarithmic compressor, it is only necessary to measure the amplitude response at one frequency step in each SFR band. Amplitude responses for the remaining frequency channels are derived from this amplitude response by using the results from the channel-to-channel gain test (see next section). This combination of calibrations is sufficient to determine the input signal strength for all frequency steps in each SFR band.

5.2. Frequency Response and Phase Calibrations

Frequency response and phase calibration tests were performed simultaneously by applying an input signal of fixed amplitude and sweeping from the lowest frequency to the highest frequency. For parallel receivers that simultaneously receive signals from two antennas, the phase difference in degrees was measured using the same input signal to both receiver inputs. The measured phase values were assembled in a phase calibration table for each receiver.

Figure 9 shows the frequency response of the five SFR channels. This plot provides the channel-to-channel gain relationship that is used to calibrate the amplitude response across channel boundaries. Similar channel-to-channel gain plots were created for the MCA channels. A combination of amplitude response and frequen-

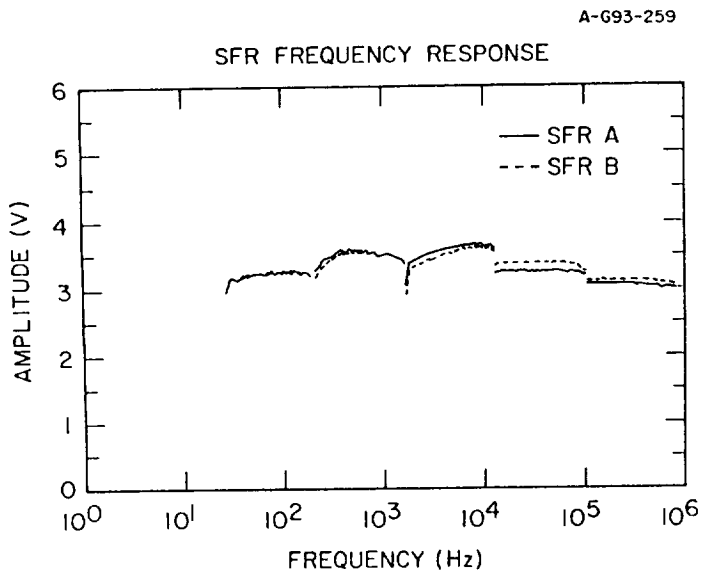

Fig. 9. The frequency response plot for the five SFR bands. The frequency response test gives the channel-channel-gain adjustment, which is used to calibrate a fixed-amplitude signal for the SFR frequency steps within a given frequency band and to calibrate a fixed-amplitude signal across channel boundaries.

cy response measurements are used to create a complete set of calibration look-up tables for each receiver. In the case of the SFR receivers, the channel-to-channel gain measurements provide the necessary adjustments to create a complete set of calibration tables for every SFR frequency step.

To verify that the amplitude and frequency response of each filter are independent of temperature, all of the above tests were conducted at room temperature (25 °C), at 0 °C, and at 40 °C.

Because the electric antennas were constructed and calibrated by the EFI team, all tests prior to spacecraft integration were performed by applying the input signals directly to the main instrument package. A similar procedure was used for the magnetic antennas. To obtain frequency response and phase calibrations for the sensor-receiver system, tests were independently performed on the sensors and combined with the calibrations for the main electronic package. In addition, prelaunch end-to-end calibrations, in which the input signals were directly applied to the electric and magnetic antennas, were selectively performed to verify the in-house calibrations.

5.3. Effective Noise Bandwidths

To compute the effective noise bandwidth for the various filters used in the instruments, a white noise input signal of known spectral density (in $V^2\ Hz^{-1}$) was used.

The spectral density of the noise generator was adjusted to remain flat across the detection bandwidth of each filter. The DC output of the log compressor was then compared to the corresponding output for a sine wave stimulus (from the amplitude response calibrations). The ratio of the sine wave amplitude squared to the voltage spectral density gives the effective noise bandwidth of the filter.

5.4. Magnetic Antenna Calibrations

For the search coil and loop antennas, the magnetic field sensitivity, the frequency response, and the phase response were calibrated at the Goddard Space Flight Center Magnetic Test Facility. The transfer function measurements were performed using a large solenoid, a Helmholtz coil, and two transmitting loops, all of which were driven in various configurations by known AC current sources. The results of these four methods were compared and found to be in good agreement. The phase response was determined using a transmitting loop driven by an AC source of known phase. The magnetic noise levels were measured by placing the search coil in a μ-metal container to reduce the effects of external noise sources. Figure 7 shows the estimated noise level curves for the loop and search coil antennas based on the initial examination of the calibration data.

6. Mission Operations

During the operational phase of the Polar mission, the PWI modes of operation will be altered several times per orbit to optimize the data return and to meet scientific objectives. The PWI instrument offers a great deal of flexibility in the selection of operational modes. In the survey mode of operation, each receiver will be set to a pre-defined default mode with an optimal sensor configuration to meet the scientific objectives of the mission. The features of the default modes, the antenna selection, and the receiver configuration are listed in Table VII.

Low-rate data from the instrument will be collected on the spacecraft tape recorder for later transmission to the ground during scheduled tape recorder dumps. Occasionally, the HFWR will be commanded in a special mode in which the waveform data are transmitted directly to the ground-tracking stations via the 256 kb s^{-1} wideband link. This high-rate waveform mode of the HFWR is only used for the real-time transmission of pre-selected waveform receiver data and will take the place of normal wideband data transmission.

Once the initial testing period has been completed, the WBR will operate on a 15% duty cycle, allowing 3.6 hr of real-time data transmission per day via the 256 kb s^{-1} data downlink. In the default mode, the 11 kHz filter and the baseband translation mode will be used to obtain high-resolution spectrums in various regions of the magnetosphere. In the WBR default mode, the 8-bit conversion mode will be used because it allows the maximum dynamic range and duty cycle for survey purposes.

TABLE VII

Default modes and antenna selections for PWI receives

Receiver	Default mode	Default frequencies	Antenna configuration	Measurements/plasma waves
SFR	Log mode	26 Hz–808 kHz	E_u/E_z	Direction finding: AKR
LFWR		5.6 Hz–10 kHz	E_v/B_u	Poynting flux: auroral hiss, AKR
MCA LFWR	6-channel	0.1 Hz–25 Hz 20 Hz–16 kHz	E_u, E_v, E_z/B_u, B_v, B_z	3-axis measurements: electromangetic ion cyclotron waves, chorus, plasmaspheric hiss
WBR	11 kHz filter 8-bit conversion mode	0 Hz–11 kHz	E_u	Survey mode to detect narrowband plasma wave features; whistlers, ion cyclotron waves, AKR spectral features

TABLE VIII
Polar PWI key parameters

Parameter	Type	Units
Epoch time (mid-piont of 5-min interval)	Real number	DD-MMM-YYYY HH:MM:SS.mmm
PB5 time (mid-point of 5-min interval)	Array of 3 integers	YY DD ms
Electron cyclotron frequency	Real number	Hz
Magnetic latitude	Real number	Degrees
Magnetic local time	Real number	Hours
Geocentric radial distance	Real number	R_E
Averages of electric field intensities	Array of 160 reals	V/m
Averages of magnetic field intensities	Array of 160 reals	nT
Peaks of electric field intensities	Array of 160 reals	V/m
Peaks of magnetic field intensities	Array of 160 reals	nT
Frequencies[a]	Array of 160 reals	Hz
SFR mode flag	Integer	0=Logarithmic 1=Linear 2=Mixed
Data quality flag	Integer	TBD
Gap flag for missing frames	Integer	Number of missing frames

[a] Constant.

Total butes per record:	2608
Total bytes in constant fields:	905
Total bytes per day:	$2608 \times 12 \times 24 = 751,104$
	$+905$
	752,009

7. PWI Key Parameters

Key parameters for the Plasma Wave Investigation will be derived from the SFR data using the E_u electric antenna and the magnetic loop antenna. Each PWI key parameter file will contain the epoch time, a real value provided by the Central Data Handling Facility and converted to time of day in units of day, month, year, hour, minute, and second. Each key parameter file will also contain 24 hours of electric and magnetic amplitudes in 160 logarithmically spaced frequencies. Both average and peak values of the electric and magnetic field amplitudes will be calculated for each 5-min interval of the day. The key parameter file will also contain the electron cyclotron frequency and selected spacecraft orbit parameters at the mid-point of each averaging interval.

A list of the PWI key parameters contained in each record is given in Table VIII. It is expected that the key parameter data will provide the user with electric and

magnetic spectrum measurements suitable for identifying events of interest. The key parameter data will be routinely available to the scientific community through the Central Data Handling Facility.

8. Summary

The Polar Plasma Wave Instrument is a complex instrument consisting of five independent receiver systems that can be connected in various configurations to seven antennas. The instrument is capable of measuring electric and magnetic field spectrums and wave vector characteristics with sufficient temporal and spectral resolution to meet the wave measurement objectives of the Polar mission. Compared to previous plasma wave instruments designed at the University of Iowa, the Polar PWI has incorporated numerous new capabilities that will refine and expand our knowledge of plasma waves in the Earth's magnetosphere, and contribute to the overall objectives of the International Solar Terrestrial Program.

Acknowledgements

This article is dedicated to the memory of the late S. D. Shawhan who was the original Principal Investigator of this investigation when proposed in 1980, to the late R. R. Shaw who was the Project Manager of the plasma wave instrument, and to the late C. K. Goertz who was a Co-Investigator.

The authors extend their thanks to the personnel of the University of Iowa Electronics and Machine Shops who fabricated the PWI; to the University of Iowa software engineers who developed the flight and test software: R. Brechwald, C. Herscovici, and W. Robison; to the University of Iowa engineers and technicians who designed and assembled the PWI: M. Bailey, R. Barrie, R. Beall, E. Kruse, S. Kutcher, R. Wenman, and H. Zimmon; and to the project personnel at the University of California, Berkeley, who were responsible for the design and testing of the electric antennas: P. Harvey, D. Pankow, and J. Wygant. This effort is supported by NASA contract NAS5–30371 with the Goddard Space Flight Center.

References

Burton, E. T. and Boardman, E. M.: 1933, *Proc. IRE* **21**, 1476.
Dowden, R. L.: 1959, *Nature* **184**, 803.
Ellis, G. R.: 1957, *J. Atmospheric Terrest. Phys.* **10**, 302.
Gurnett, D. A.: 1966, *J. Geophys. Res.* **71**, 5599.
Gurnett, D. A.: 1974, *J. Geophys. Res.* **79**, 4227.
Gurnett, D. A.: 1991, in C.-I. Meng, M. J. Rycroft, and L. A. Frank (eds.), *Auroral Physics*, Cambridge University Press, Cambridge, p. 241.
Gurnett, D. A. and Frank, L. A.: 1972, *J. Geophys. Res.* **77**, 172.

Gurnett, D. A. *et al.*: 1988, University of Iowa Proposal entitled 'A Plasma Wave Investigation for the NASA/GSFC Polar Mission'.
Harvey, P., Mozer, F. S., Pankow, D., Wygant, J., Maynard, N. C., Singer, H., Sullivan, W., Anderson, P. B., Pfaff, R., Aggson, T., Pedersen, A., Falthämmar, C.-G., and Tanskannen, P.: 1995, 'The Electric Field Instrument', *Space Sci. Rev.* **71**, 583 (this issue).
Kennel, C. F. and Petschek, H. E.: 1966, *J. Geophys. Res.* **71**, 1.
Laaspere, T. and Hoffman, R. A.: 1976, *J. Geophys. Res.* **81**, 524.
Louarn, P. *et al.*: 1990, *J. Geophys. Res.* **95**, 5983.
Maggs, J. E.: 1976, *J. Geophys. Res. 81*, 1707.
Martin, L. H., Helliwell, R. A., and Marks, K. R.: 1960, *Nature* **187**, 751.
Shawhan, S. D.: 1979, in L. J. Lanzerotti, C. F. Kennel, and E. H. Parker (eds.), *Solar System Plasma Physics, III*, North-Holland Publishing Co., Amsterdam, p. 211.
Shelley, E. G. and Collin, H. L.: 1991, in C.-I. Meng, M. J. Rycroft, and L. A. Frank (eds.), *Auroral Physics*, Cambridge University Press, Cambridge, p. 129.
Stix, T.: 1962, *The Theory of Plasma Waves*, McGraw-Hill, New York, p. 41.
Tonks, L. and Langmuir, I.: 1929, *Phys. Rev.* **33**, 195.
Winglee, R. M.: 1985, *Astrophys. J.* **291**, 160.
Wu, C. S. and Lee, L. C.: 1979, *Astrophys. J.* **230**, 621.
Zarka, P., LeQueau, D., and Genova, F.: 1986, *J. Geophys. Res.* **91**, 13,542.